



Precipitation Hardening in Innovative Processing of 6xxx Aluminum Alloys

A. Wimmer, A. Hämmerle, and C. D. Marioara

Abstract

Lightweight 6xxx aluminum components are the basis for a sustainable mobility. Therefore, improvements in the thermomechanical processing of 6xxx alloys are necessary to further optimize aluminum structures for the automotive market. Two optimized process routes are presented, which enhance the material's performance compared to the well-established standard process. In the first part, it is demonstrated that an elevated quenching temperature following solution heat treatment of an EN AW 6082 alloy is increasing hardness due to formation of a finer needle precipitate microstructure. TEM imaging showed that the unused solute in-between the needles were clustered, which was calculated to provide an additional hardness contribution. In the second part, a large-scale T8 process involving impact extrusion and artificial aging of an EN AW 6060 alloy was optimized for a favorable combination of strength and ductility. In this case, the properties were the result of work hardening and preferred precipitation on dislocations.

Keywords

Aluminum • Thermomechanical processing • Precipitation hardening • TEM • Quench rate • Impact extrusion

Introduction

The main strengthening mechanism in conventional Al–Mg–Si(–Cu) alloys (6xxx) is precipitation hardening. The full thermomechanical processing of these materials is complex and depends on the application. However, for most applications, the crucial process steps are similar and begin with solutionizing, followed by a rapid cooling. In order to avoid detrimental quench-induced precipitation, which reduces the full age-hardening potential of the alloy, a critical cooling rate must be ensured [1]. After quenching, soluble elements together with a high concentration of quenched-in vacancies are in supersaturated solid solution of the face-centered cubic (fcc) parent lattice of aluminum [2]. Out of this supersaturated solid solution, atomic clusters form even at room temperature (RT) [3, 4]. Two types of clusters have been identified, based on their influence on the subsequent microstructure development during artificial aging (AA). One is a detrimental, “bad” cluster which delays the nucleation and growth of β , the main hardening phase in this system [5, 6]. For high alloyed 6xxx alloys such as EN AW 6082, with a total (Mg + Si) content above approx. 1 wt%, these “bad” cluster form when the material is stored at RT before aging [7, 8]. Another is a beneficial, “good” cluster type (also called ‘Cluster 2’) which was measured to form at temperatures above approx. 70 °C [9, 10]. For lean 6xxx alloys such as EN AW 6060, with a total (Mg + Si) content below approx. 1 wt%, with prolonged prior storage at RT a higher strength during AA can be reached [11, 12] due to formation of “good” clusters. Based on these observations, the question arises whether an improvement of strength in a dense EN AW 6082-type alloy during AA can be obtained by modifying the temperatures of the quenching media combined with a short holding time. This is one part of the present work. Also, once the needle precipitate microstructure was measured by TEM, its hardness contribution was calculated, and the total hardness was compared to the experimental value. In particular, it has been previously

A. Wimmer (✉) · A. Hämmerle
Neuman Aluminium Industries, Werkstraße 1, 3182 Marktl,
Austria
e-mail: alexander.wimmer@neuman.at

C. D. Marioara
SINTEF Industry, Høgskoleringen 5, 7465 Trondheim, Norway

measured by TEM and atom probe tomography (APT) that large amounts of solute in dense alloys are not utilised in needle precipitate formation up to peak hardness [13, 14]. Therefore, in our work, we investigated if this solute, left in between the main needle-type precipitates was clustered, in which case it would contribute to the total strength more than if it had been in a solid solution.

In addition to cooling rates from extrusion or SHT and quench temperature and holding time prior to AA, another important aspect is the process sequence. In our investigated T8 process route, the material is deformed after solution heat treatment but before AA, hence high deformation forces are required and dislocations are introduced into the Al matrix. The dislocations become preferred nucleation sites for needle precipitates during AA. In this case the final hardness is given by a combination of work hardening and precipitation hardening [15, 16]. This interplay is complex, as the contribution from dislocations and precipitates differ depending on the deformation level and AA temperature and time. In addition to hardness, ductility is another important parameter in applications. It decreases with increasing deformation level and precipitation hardening. Therefore, in our second example, we demonstrate the possibility to achieve an acceptable compromise of strength and ductility in an impact extrusion process by changing the process order and by optimization of temperature and holding time during the subsequent AA.

Experimental Details

For quenching experiments, an EN AW 6082 alloy with 1.30 wt% Si, 1.00 wt% Mg, 0.70 wt% Mn, 0.19 wt% Fe, 0.19 wt% Cr, and 0.08 wt% Cu was studied. Flat, dog bone-shaped samples with a thickness of 3 mm were solutionized for 60 ± 5 min at 813 ± 10 K and afterwards quenched. Different quench rates were realized using air and water quenching, with an air speed between 0.1 m/s (natural, convective flow) and 3 m/s (using a ventilation system) and water temperatures of 293 K (cold water), 323 K (warm water), and 363 K (hot water). The quench rate was measured with thermocouples, which were attached at the sample surface. Samples were naturally aged for 2 h (transfer time between quench and artificial aging). Artificial aging (AA) was performed at 433 K for 14 h to reach T66 (peak-aged) condition.

For deformation experiments, the alloy EN AW 6060 was impact extruded in the soft annealed (T6 process) and cold water-quenched condition (T8 process). The 6060 alloy had a chemical composition of 0.47 wt% Si, 0.38 wt% Mg, 0.05 wt% Mn, 0.23 wt% Fe, 0.01 wt% Cr, and 0.02 wt% Cu. EN AW 6082 has not been used as DEFORM simulations indicated that due to the high deformation resistance the

temperature increase during deformation would be approx. 200 °C, resulting in over-aging and dislocation annihilation. Cylinder-shaped samples (90 mm diameter, 42 mm height) were impact extruded under adiabatic conditions (deformation time approx. 0.1 s) to a cup with an outer diameter of 90 mm and a wall thickness of 4 mm. Afterwards, artificial aging (AA) was performed for 4 h at 413 K (severe under-aged condition), 14 h at 413 K (under-aged condition), and 8 h at 433 K (under-aged condition).

Hardness tests were carried out on a “KB Prüftechnik” hardness tester and tensile tests were done on a “Zwick Universal Prüfmaschine Z100”. TEM analysis was performed on a LaB₆ filament JEOL 2100 TEM operated at 200 kV and equipped with a Gatan Imaging Filter. Electron Energy Loss Spectroscopy (EELS) was used for thickness determination, which was approx. 100 nm for the analyzed volumes. As the metastable needle precipitates are parallel to $\langle 100 \rangle$ Al directions, the TEM images used for their quantification were recorded in this zone axis. Needle precipitate parameters (number density, length, cross-sectional area, and volume fraction) were calculated using the methodology described in [17]. Up to 250 needle lengths were measured from eight to ten bright-field images and between 4000 and 6000 needle cross sections were counted from the corresponding dark-field images for volume density determination. Up to 250 needle cross-sectional areas were measured from another set of bright-field images recorded at higher magnifications. Cluster densities were estimated by counting the bright, round-shaped particles observed in-between the needle precipitates and the dark cross sections in the higher magnification bright field TEM images.

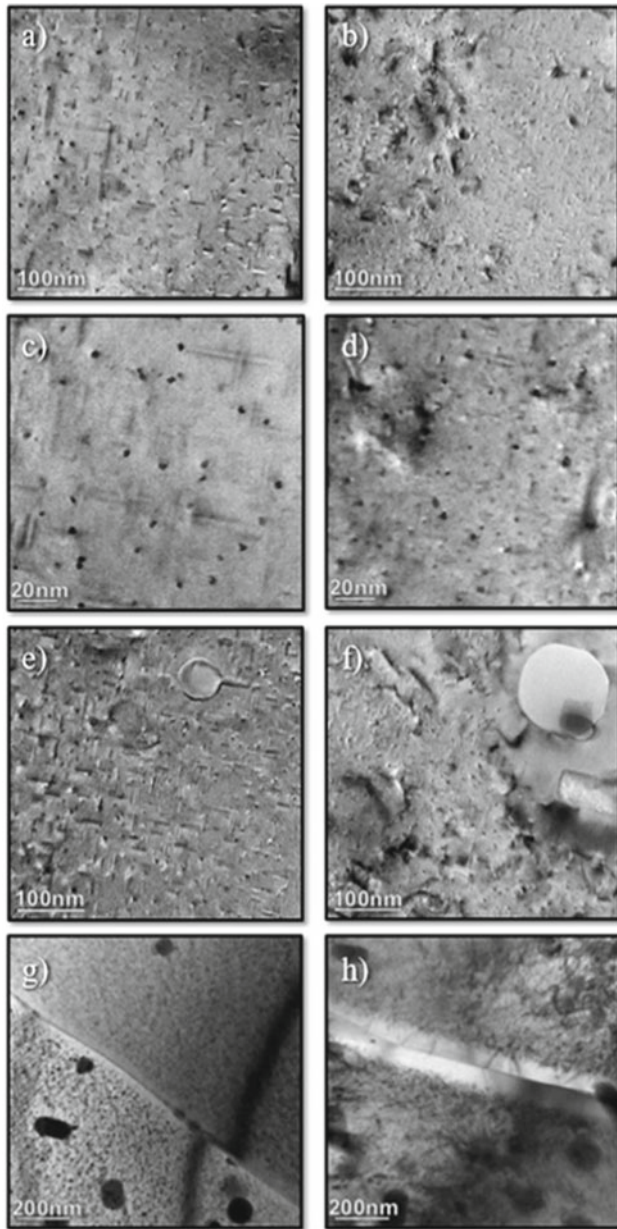
Results and Discussion

Quenching Experiments of EN AW 6082

The quench rate of the quenching experiments and the obtained yield stress (YS) are shown in Table 1. It can be seen, that the quenching rate was between 2 K/s and 250 K/s, resulting in a YS of 165–342 MPa. The samples with 293 K and 363 K water quench were further analyzed in the TEM (Fig. 1). Figure 1a shows the microstructure of the 293 K-quenched samples, Fig. 1b displays the 363 K-quenched samples. In the 363 K samples, much more, finer β'' -needles are visible, precipitation statistics are shown in Table 2. By using the precipitation statistics of Table 2 and Eq. (14) in Ref. [5], it is possible to calculate a strength contribution from precipitates (β'' -needles) σ_{prec} of 166 MPa for 293 K samples and 244 MPa for 363 K samples. As only approx. 1/3 of the Mg and Si is precipitated as β'' -needles, the level of Mg and Si in solid solution (SSSS) remains significant (Table 3). By using these numbers and

Table 1 Quench rate and yield stress σ_{meas} as a function of quenching media

Quench media	Quench rate (K/s)	σ_{meas} (MPa)
water, 293 K	250	313
water, 323 K	240	338
water, 363 K	100	342
air, 3 m/s	9	269
air, 1 m/s	4	214
air, 0.1 m/s	2	165

**Fig. 1** TEM bright-field images, the left column (a, c, e, and g) depicts the samples quenched with water, 293 K, the right column (b, d, f, and h) depicts the samples quenched with water, 363 K. From a and b, the β'' -needle characteristics are observed and c and d show clusters (light grey spots). PFZ width is determined with e and f (at dispersoids) as well as g and h (at grain boundaries)

Eq. (5–7) in Ref. [5], a solid solution strengthening contribution σ_{ss} of 46 MPa for 293 K samples and 49 MPa for 363 K samples can be calculated. However, at higher magnifications, clusters are getting visible in the TEM images (Fig. 1c and d). While the dark spots are affiliated to β'' -needles, it is assumed that the grey/bright spots can be attributed as clusters. If a TEM sample thickness of approx. 100 nm is estimated, an average distance between clusters of 10 nm for 363 K and 20 nm for 293 K condition has been calculated, resulting in the cluster statistics shown in Table 4. As cluster density was only approximated from TEM images, APT analysis will be performed to get deeper insights about cluster statistics. Based on Eq. (14) in Ref. [5] the strength contribution from clusters σ_{clus} is estimated to be 27 MPa for 293 K samples and 85 MPa for 363 K samples. However, it has to be considered that in case of existence of clusters the level of Mg and Si in solid solution will be lower, resulting in a lower contribution of solid solution strengthening. Strength contribution from dispersoids σ_{disp} (total dispersoid volume fraction approx. 0.3%), calculated based on Eq. (12) in Ref. [5], is estimated in the order of 30 MPa. As samples were in the undeformed condition, dislocation hardening/work hardening is expected to be 0. With the internal yield stress σ_i , which should be in the order of 10 MPa [5, 18], it is now possible to calculate the overall theoretical yield stress σ_{theo} (Table 5). For the 293 K samples, the theoretical yield stress σ_{theo} is expected to be 243–279 MPa (243 MPa if solid solution and cluster strengthening are counted 50% each, 279 MPa if solid solution and cluster strengthening are counted 100% each). For the 363 K samples, the theoretical yield stress σ_{theo} is expected to be 350–418 MPa. Comparing these theoretical values with the obtained yield stress in the tensile test, the yield stress for 293 K samples is under-estimated while it is over-estimated for the 363 K samples. On the one hand, uncertainties can be explained by the rough estimate of cluster densities, on the other hand, solid solution strengthening is over-estimated as some of the Mg and Si in solid solution precipitated as clusters. Finally, the width of the precipitation-free zone (PFZ) on dispersoids (Fig. 1e and f) and on grain boundaries (Fig. 1g and h) is significantly larger for the 363 K samples compared to the 293 K

Table 2 Precipitation statistics for β'' -needles in 293 K and 363 K quenched samples and calculated precipitation strengthening σ_{prec}

Condition/Parameter	Needle density (μm^{-3})	Needle length (nm)	Needle cross section (nm^2)	Needle volume fraction (%)	σ_{prec} (MPa)
6082_293K	$79,232 \pm 8,296$	22.11 ± 0.68	5.38 ± 0.20	0.943 ± 0.121	166
6082_363K	$221,890 \pm 22,511$	10.13 ± 0.23	3.31 ± 0.10	0.743 ± 0.086	244

Table 3 Remaining Mg and Si content in solid solution and calculated solid solution strengthening σ_{ss} . For calculation of Mg and Si in solid solution, it has been assumed that β'' -needles consist of $\text{Mg}_5\text{Al}_2\text{Si}_4$

Condition/Parameter	Needle volume fraction (%)	Mg in SSSS (at%)	Si in SSSS (at%)	σ_{ss} (MPa)
6082_293K	0.943 ± 0.121	0.723	0.786	46
6082_363K	0.743 ± 0.086	0.806	0.852	49

Table 4 Precipitation statistics for clusters in 293 K- and 363 K-quenched samples and calculated cluster strengthening σ_{clus}

Condition/Parameter	Cluster density (m^{-3})	Guinier radius r_G (nm)	σ_{clus} (MPa)
6082_293K	$\approx 10^{23}$	≈ 1.3 [8]	27
6082_363K	$\approx 10^{24}$	≈ 1.3 [8]	85

Table 5 Calculation of the theoretical yield stress σ_{theo}

Condition/Parameter	σ_{prec} (MPa)	σ_{ss} (MPa)	σ_{clus} (MPa)	σ_i (MPa)	σ_{disp} (MPa)	σ_{theo} (MPa)	σ_{meas} (MPa)
6082_293K	166	46	27	10	30	243–279	313
6082_363K	244	49	85	10	30	350–418	342

samples. For 363 K samples, PFZ on the grain boundaries and around dispersoids was approx. 200 nm, compared to 100 nm for 293 K samples. As the PFZ is consisting of 99.5% pure aluminum, the PFZ is not significantly contributing to strength and consequently, if the PFZ becomes larger, the measured yield strength in the tensile test is decreasing.

It is remarkable that, in the T66 (peak-aged) condition, only approx. 1/3 of the Mg and Si atoms are precipitated as β'' -needles, however, contributing 50–70% to the yield stress of the material. The remaining 2/3 of Mg and Si atoms are still in solid solution or clusters, contributing to about 30% of the overall yield stress.

Deformation Experiments of EN AW 6060

Five conditions were characterized:

- Soft anneal, impact extrusion, solutionizing, quench, 14 h aging at 433 K (T6)
- Solutionizing, quench, impact extrusion (T8, as-pressed)
- Solutionizing, quench, impact extr., 4 h aging at 413 K (T8, 4 h@413 K)

- Solutionizing, quench, impact extr., 8 h aging at 433 K (T8, 8 h@433 K)
- Solutionizing, quench, impact extr., 14 h aging at 413 K (T8, 14 h@413 K)

As in the T6 route a SHT is performed just before AA, most of the dislocations introduced during impact extrusion are annealed out, and precipitation occurs in an undeformed matrix. However, in the T8 route the impact extrusion takes place between SHT and AA, and only part of the introduced dislocations are annealed out. In this case, precipitation during AA takes place in a deformed matrix. Both T6 and T8 materials were subjected to mechanical characterization, and the results are shown in Fig. 2. It can be seen, that the T6 condition has an elongation to fracture ϵ_f of 18%, which is significantly higher compared to 10% of the T8 as-pressed condition. However, if the T8 material is artificially aged, ductility is increasing to approx. 13%. While ductility in the T8 condition is never as high as in the T6 condition, the yield stress and ultimate tensile stress in T8 condition are exceeding the T6 condition significantly. After artificial aging for 4 h at 413 K, the growth of precipitates is not yet advanced enough for significant hardness contributions, however, after 8 h at 433 K dislocation annihilation has

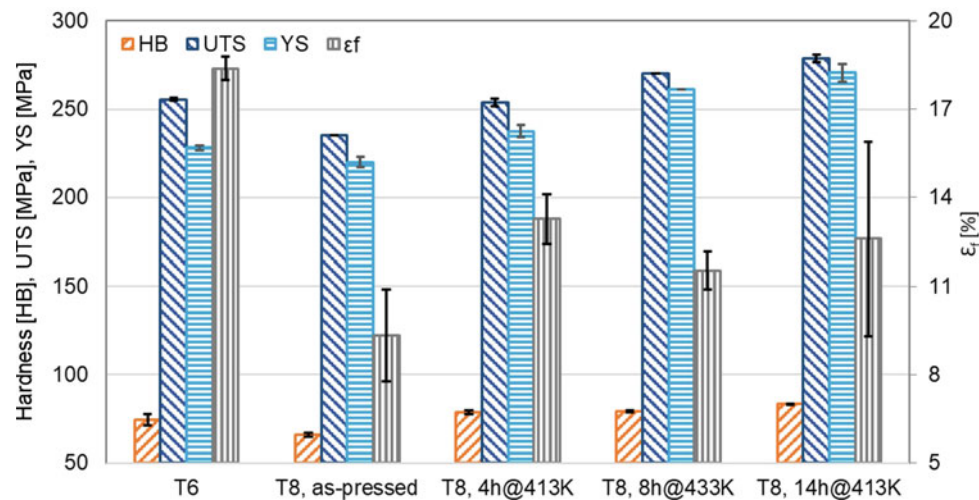


Fig. 2 Mechanical properties in the T6 and different T8 conditions

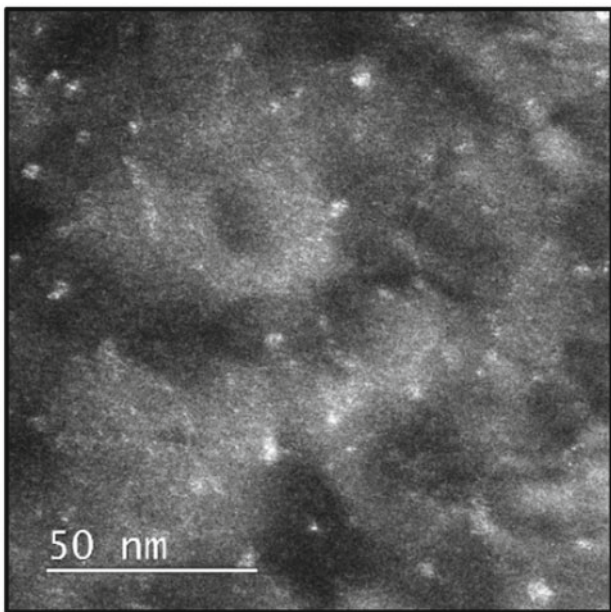


Fig. 3 T8 condition after 4 h aging at 413 K (T8, 4 h@413 K). Bright spots show the cluster distribution, especially alongside dislocation lines

progressed too far. Subsequently, an artificial aging of 14 h at 413 K provides the best compromise between the desired growth of precipitates and the undesired extinction of dislocations. Especially the yield stress, the most important design parameter, is 20% higher for the “T8, 14 h@413 K” condition compared to the classical T6 condition. An explanation for the superior mechanical properties can be found in TEM images of the T8 condition in Fig. 3. Here we see a high density of small clusters or precipitates that are formed on dislocation lines during the AA. During

deformation, these clusters act as obstacles for the new dislocations, resulting in a higher dislocation density and formation of dislocation cells, which have been associated with increased ductility [16].

Conclusion

Two improved thermomechanical processing routes for 6xxx aluminum alloys are presented, which give superior mechanical properties as compared to conventional procedures. In one case, the hardness of an extruded EN AW 6082 alloy is increased by controlling the cooling rate and quench temperature after SHT. In the other case, strength and ductility of an EN AW6060 alloy, processed by impact extrusion, is optimized by changing the process sequence and AA temperature and holding time.

In the first case, based on TEM observations and the obtained precipitation and cluster statistics the theoretical yield stress contributions have been calculated. A significant influence of clusters on the yield stress has been found. Despite a much wider PFZ, the hot water-quenched samples showed a 10% higher yield stress compared to cold water-quenched samples due to a three times higher β'' -needle density and also significant higher cluster density in T6 condition. This illustrates that the influence of clusters has so far been given too little importance.

A fast, almost adiabatic T8 process has been developed, which is utilizing dislocation hardening, cluster and precipitation hardening in parallel, resulting in a yield stress 20% higher compared to a classical T6 process. It has been shown that at an aging temperature of 413 K precipitation hardening combined with a low dislocation annihilation rate can be forced, with the result of an optimized combination of

strength and ductility. The optimum combination of strength and ductility is particularly important for safety components and enables high wear resistance.

Acknowledgements The authors thank the Austrian Research Promotion Agency FFG for their financial support (FFG project numbers 853869 and 887078).

References

- Milkereit B, Starink MJ, Rometsch PA, Schick C, Kessler O (2019) Review of the Quench Sensitivity of Aluminium Alloys: Analysis of the Kinetics and Nature of Quench-Induced Precipitation, *Materials* 12(24):4083
- Lang P, Povoden-Karadeniz E, Mayer W, Falahati A, Kozeschnik E (2013) The Bustling Nature of Vacancies in Al Alloys. In: Marquis F. (eds) *Proceedings of the 8th Pacific Rim International Congress on Advanced Materials and Processing*. Springer, Cham.
- Røyset J, Stene T, Sæter JA, Reiso O (2006) The Effect of Intermediate Storage Temperature and Time on the Age Hardening Response of Al-Mg-Si Alloys, *Mat Sci Forum* 519-521:239-244
- Pashley D, Rhodes J, Sendorek A (1966) Delayed ageing in Aluminium-Magnesium-Silicon alloys - effect on structure and mechanical properties, *Journal of the Institute of Metals* 94 (2):41-49
- Engler O, Schäfer C, Myhr OR (2015) Effect of natural ageing and pre-straining on strength and anisotropy in aluminium alloy AA 6016, *Materials Science and Engineering A* 639:65-74
- Engler O, Marioara CD, Aruga Y, Kozuka M, Myhr OR (2019) Effect of natural ageing or pre-ageing on the evolution of precipitate structure and strength during age hardening of Al-Mg-Si alloy AA 6016, *Materials Science and Engineering A* 759:520-529
- Aruga Y, Kim SN, Kozuka M, Kobayashi E, Sato T (2018) Effects of cluster characteristics on two-step aging behavior in Al-Mg-Si alloys with different Mg/Si ratios and natural aging periods, *Materials Science and Engineering A* 718(7):371-376
- Hämmerle A, Wimmer A (2021) The impact of natural aging in Al-Mg-Si alloys and influence of Sc contributions, Paper presented at the Euromat conference, online, 13–17 September 2021
- Nosedá Grau V, Cuniberti A, Tolley A, Castro Riglos V, Stipcich M (2016) Solute clustering behavior between 293K and 373K in a 6082 Aluminum alloy, *Journal of Alloys and Compounds* 684:481-487
- Serizawa A, Hirose S, Sato T (2008) Three-dimensional atom probe characterization of nanoclusters responsible for multistep aging behavior of an Al-Mg-Si alloy, *Metallurgical and Material Transactions A* 39(2):243-251
- Chang CS, Wieler I, Wanderka N, Banhart J (2009) Positive effect of natural pre-ageing on precipitation hardening in Al-0.44at% Mg-0.38at% Si alloy, *Ultramicroscopy* 109(5):585–592
- Stamenkovic U, Ivanov S, Markovic I, Mladenovic S, Manasijevic D, Balanovic L (2019) The influence of natural aging and pre-ageing on the mechanical, physical and microstructural properties of the EN AW-6060 aluminium alloy, *Machines. Technologies. Materials* 13:187-189
- Engler O, Schäfer C, Brinkman HJ, Marioara CD, Kozuka M, Shishido H, Aruga Y (2017) A combined TEM and atom probe approach to analyse the early stages of age hardening in AA 6016, *Materials Science Forum* 877:231-236
- Aruga Y, Kozuka M, Takaki Y, Sato T (2014) Evaluation of solute clusters associated with bake-hardening response in isothermal aged Al-Mg-Si alloys using a three-dimensional atom probe, *Metallurgical and Materials Transactions A* 45:5906-5913
- Teichmann K, Marioara CD, Andersen SJ, Marthinsen K (2012) The effect of preaging deformation on the precipitation behavior of an Al-Mg-Si alloy, *Metallurgical and Material Transactions A* 43:4006-4014
- Qvale K, Hopperstad OS, Reiso O, Tundal UH, Marioara CD, Borvik T (2021) An experimental study on pre-stretched double-chamber 6000-series aluminium profiles subjected to quasi-static and dynamic axial crushing, *Thin-Walled Structures* 158:107160
- Marioara CD, Andersen SJ, Zandbergen HW, Holmestad R (2005) The influence of alloy composition on the precipitates of the Al-Mg-Si system, *Metallurgical and Materials Transactions A* 36:691-702
- Sumomogi T, Yoshida M, Yoshida M, Nakamura M, Nakamura M, Osono H, Kino T (2004) Mechanical Properties of Ultra High-Purity Aluminum, *J Japan Institute of Metals* 68(11):958-964